

---

# Property of Young Massive Clusters in a Galaxy-Galaxy Merger Remnant

Hidenori Matsui<sup>1,2</sup>, Ataru Tanikawa<sup>2,3</sup>, and Takayuki R Saitoh<sup>4</sup>

<sup>1</sup>National Institute of Technology, Asahikawa College, Asahikawa, Shunkodai 2-2-1-6, Asahikawa, Hokkaido, 071-8142, Japan

<sup>2</sup>Department of Earth Science and Astronomy, College of Arts and Sciences, The University of Tokyo, 3-8-1 Komaba, Meguro-ku, Tokyo, 153-8902, Japan

<sup>3</sup>RIKEN Advanced Institute for Computational Science, 7-1-26 Minatojima-minami-machi, Chuo-ku, Kobe, Hyogo 650-0047, Japan

<sup>4</sup>Earth-Life Science Institute, Tokyo Institute of Technology, 2-12-1, Ookayama, Meguro, Tokyo, 152-8551, Japan

\*E-mail: matsui@asahikawa-nct.ac.jp

Received (reception date); Accepted (acceptation date)

## Abstract

We investigate the properties of young massive clusters (YMCs) in a galaxy-galaxy merger remnant by analyzing the data obtained by a gas rich major merger simulations in Matsui et al. 2012. We found that the YMCs are distributed at a few kpc and at  $\sim 10$  kpc from the galactic center, in other words, there are two components of their distribution. The former are formed in filamentary and turbulent gas generated at a few kpc from the center because of galaxy encounters, and the latter are formed in tidal tails which are far from the center. The YMCs are much less concentrated than galaxy stars. The mass function of the YMCs is  $dN/dM \propto M^{-2}$ . Most of YMCs are formed from the second encounter to the final coalescence phase of the galactic cores, and their formation rate is especially high at final coalescence phase. Most of them consists of single stellar population in age, but YMCs with multi stellar populations in age are also formed. The multiple populations are produced by the following process: a YMC captures dense gas, and another generation stars form within the cluster. There are several YMCs formed in an isolated disk before the encounter of galaxies. These candidates contain stars with various age by capturing dense gas and forming stars. YMCs in a merger remnant, have various orbits, but large fraction of candidates have circular orbits.

**Key words:** methods: numerical — galaxies: evolution — galaxies: formation — galaxies: interactions — galaxies: structure

---

## 1 Introduction

Major mergers of gas-rich galaxies are expected to play an important role in formation of globular clusters. The CO observation of local interacting galaxies showed a compressed gas filament, which may lead to formations of globular clusters, induced by galaxy-galaxy collision (Kaneko et al. 2018). The optical and infrared images

found young massive star clusters with  $\sim 10^{5-6} M_{\odot}$  formed in galaxy-galaxy merging process (Whitmore & Schweizer 1995; Whitmore et al. 1999; Mengel et al. 2008). In galaxy-galaxy merger remnants, globular cluster systems formed in a galaxy-galaxy merging process are detected (Bassino & Caso 2017; Ko et al. 2018). In order to study formation, evolution, and properties of such globular cluster systems in more detail, numerical simulations of a galaxy-galaxy

merger are needed.

Previously, a large number of numerical simulations of the galaxy mergers have been performed (Mihos & Hernquist 1996; Barnes & Hernquist 1996; Kazantzidis et al. 2005; Cox et al. 2006; Di Matteo et al. 2007). These numerical simulations succeeded to understand roughly dynamics in galaxy-galaxy merging process such as gas inflow to the galactic central region or a central starburst. These studies, however, were difficult to reproduce shock-induced star and star cluster formations in the merging process as shown by observations. This is because they used unrealistic interstellar medium (ISM) model with temperature cutoff at  $T = 10^4$  K in a cooling function due to the limited mass and spatial resolution. The artificial high temperature floor of ISM prevents ISM from gravitational instability at the shock generated by the galaxy-galaxy encounter.

In order to investigate formations of star clusters in galaxy-galaxy merging process, subgrid model for star clusters is used instead of resolving formations of individual star clusters directly (Bekki et al. 2002; Kruijssen et al. 2012). Bournaud et al. (2008) have performed high-resolution simulations of merging galaxies and reproduced formations of star clusters directly, although they used method of sticky particles instead of resolving hydrodynamics.

Recently, the higher mass and spatial resolution simulations of merging galaxies have been performed (Saitoh et al. 2009; Kim et al. 2009; Teyssier et al. 2010; Matsui et al. 2012; Hopkins et al. 2013a; Hopkins et al. 2013b; Renaud et al. 2015). The high resolution simulations allow us to take radiative cooling of low temperature gas ( $T < 10^4$  K) into account and realize multi-phase nature of ISM. These simulations have naturally succeeded to reproduce shock-induced star and star cluster formations. These studies have clarified shock-induced star cluster formations at the first encounter of galaxies (Saitoh et al. 2009; Saitoh et al. 2010), formations of hypermassive star clusters in galaxy-galaxy merging process (Matsui et al. 2012), and formation mechanism of star cluster at each interaction stage (Renaud et al. 2015). The formation of globular clusters in merging galaxies at high-redshift are also clarified by cosmological simulations (Kim et al. 2018). Although formations of star clusters in the merging process were clarified, properties of globular clusters in a merger remnant have not been analyzed yet.

In this paper, we focus on and investigate properties of young massive cluster (YMCs) formed in galaxy-galaxy merging process, which can produce luminous infrared galaxies (LIRGs) as shown in paper I. For this purpose, we analyze a galaxy-galaxy merger remnant obtained by

Matsui et al. (2012) (hereafter paper I). We describe our methods in §2 and results in §3. Summary and discussions are presented in §4.

## 2 Method

### 2.1 Simulation data

To investigate a merger remnant and YMCs in the remnant, simulation data obtained by paper I is analyzed. Here, the simulations have been performed by Tree+GRAPE SPH/N-body code “ASURA” (Saitoh et al. 2008). We analyze mainly the data of the highest resolution model called  $H_{\text{TT},5\text{pc}}$ . In this model, initial setup is as follows. Firstly, we simulate an isolated disk galaxy, which consists of an exponential disk with  $6.3 \times 10^9 M_{\odot}$  and a dark matter halo with  $1.1 \times 10^{11} M_{\odot}$ , for 1000 Myr. The initial disk and halo include gas, of which metallicity is 0.01, with  $1.2 \times 10^9 M_{\odot}$  and  $1.1 \times 10^9 M_{\odot}$ , respectively. The initial metallicity is slightly less than solar metallicity and larger than that of large magellanic cloud (Choudhury et al. 2016). After stabilizing the disk, we start galaxy-galaxy merger simulations in which both disks are tilted at  $-109^{\circ}$  and  $71^{\circ}$  to the orbital plane, respectively, and prograde-prograde encounter occurs. We set the time of starting the merger simulation to be  $t = 0$ . At  $t = 0$ , each galaxy includes gas with  $1.5 \times 10^9 M_{\odot}$  since gas decreases due to star formation. Hereafter, initial stars at  $t = -1000$  Myr, newly born stars before  $t = 0$ , and after  $t = 0$  are called “pre-existing stars”, “old stars”, and “new stars”. After starting the merger simulation, the first, second, and third encounters occur at  $t \sim 450$  Myr,  $t \sim 850$  Myr, and  $t \sim 1000$  Myr, respectively. See paper I in details.

In the  $H_{\text{TT},5\text{pc}}$  model, the particle numbers of SPHs, pre-existing and old stars, and dark matter at  $t = 0$  are 442958, 2051314, and 27720000, respectively. The mass and gravitational softening length of SPH particles are  $7.5 \times 10^3 M_{\odot}$  and 5 pc, respectively. In the simulation, multi-phase nature of ISM are realized by taking a wide temperature range of radiative cooling ( $10 \text{ K} < T < 10^8 \text{ K}$ ) and energy feedback from Type II supernovae (SNe) into account. Metal contamination of gas by Type II SNe is also taken into account (Steinmetz & Mueller 1994). Star formations take place from cold ( $T < 100 \text{ K}$ ) and dense ( $n_{\text{H}} > 100 \text{ cm}^{-3}$ ) gas. The mass of a star particle spawned from an SPH is one third of SPH mass.

In addition to model  $H_{\text{TT},5\text{pc}}$ , the lower resolution models  $H_{\text{TT}}$  and  $L_{\text{TT}}$  are also analyzed. These models have different mass and spatial resolutions from model  $H_{\text{TT},5\text{pc}}$ , but same collision parameter. In  $H_{\text{TT}}$  model, the gravi-

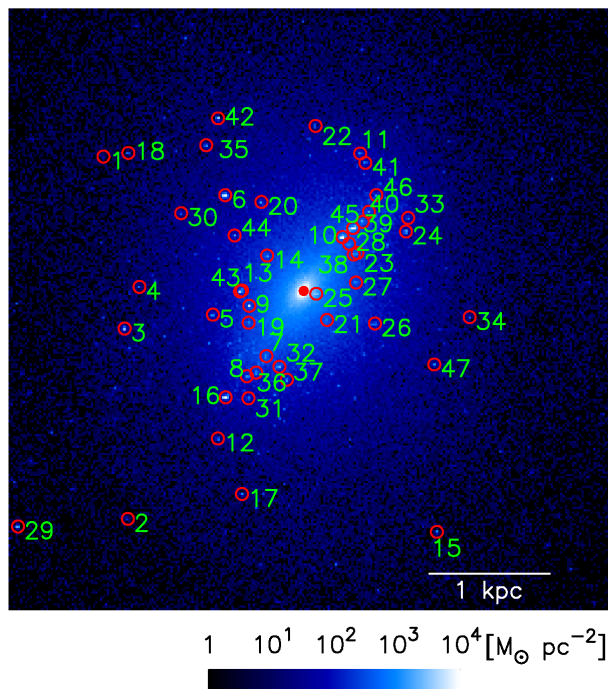


**Fig. 1.** Snapshot of both new stars and old stars in a merger remnant. The size of the panel is 5 kpc. The colors represent surface density of both new stars and old stars. A filled and open circles denote the galactic center and detected YMCs. The numbers around the YMCs show ID of clusters. Although some faint dots can be observable in the other points, these objects cannot be identified as YMCs since they are gravitationally unbound or cluster mass does not reach the detection limit mass. Two YMCs are not seen in this figure since these are much far from the galactic center.

tational softening length is 20 pc but same SPH mass as  $H_{TT,5pc}$ . In  $L_{TT}$  model, SPH mass is  $3 \times 10^4 M_{\odot}$ , and gravitational softening length is 20 pc.

## 2.2 Identification of young massive clusters

We analyze simulation data at  $t \sim 1350$  Myr. At that time, about 300 Myr passes after the galaxy merger is completed. We regard lower limit of detectable mass of the cluster as  $2 \times 10^5 M_{\odot}$  in  $H_{TT,5pc}$  and  $H_{TT}$  and as  $8 \times 10^5 M_{\odot}$  in  $L_{TT}$ , since clusters can be expressed by 100 new star particles.

In order to detect YMCs, we firstly compute the gravitational potential energy of old and new stars. After the calculation, we perform gravitational bound check for old and new star particles around the particle with locally minimum potential. If particles are gravitationally bound and the total mass of the bound particles exceed the mass limit, we identify the system as a YMC.

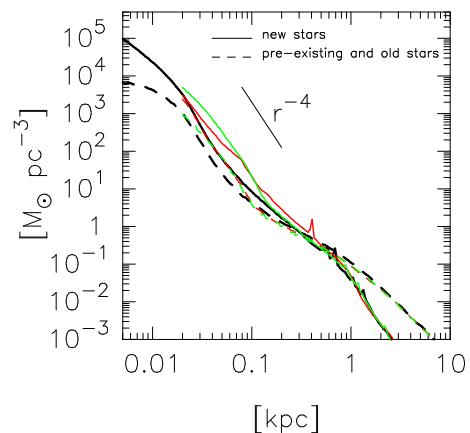


**Fig. 2.** Density profiles of young stars (solid lines) and pre-existing and old stars (dashed lines) in the merger remnants. Black, red, and green lines show simulation models of  $H_{TT,5pc}$ ,  $H_{TT}$ , and  $L_{TT}$ , respectively. The red and green lines are not drawn within 20 pc since gravitational softening length, namely spatial resolution, is 20 pc.

## 3 Results

### 3.1 Merger remnant

Snapshot of a merger remnant at  $t \sim 1350$  Myr in  $H_{TT,5pc}$  model is shown in figure 1. We detect 49 YMCs in the remnant.

Figure 2 shows the density profile of new stars and pre-existing and old stars in the merger remnant at  $t \sim 1350$  Myr. The density profile of new stars is steep and declines as approximately  $\rho \propto r^{-4}$  in outer region larger than several ten parsec. The profile with  $r^{-4}$  is produced by experience of strong gravitational disturbances (Makino et al. 1990). In the case of a galaxy merger, the intense disturbances are caused by merging of galactic cores and sink of hypermassive star clusters through dynamical friction. Within 500 pc from the galactic center, new stars are dominant. The central density is much higher than that of both pre-existing and old stars by one order of magnitude. Such structures are compatible with extremely compact structures of newly formed stars observed in ultraluminous infrared galaxies (ULIRGs) (Soifer et al. 2000; Mao et al. 2014).

The merger remnant has the total stellar mass of  $1.2 \times 10^{10} M_{\odot}$  at that time.  $V$ -band absolute magnitude  $M_V$  of the remnant is estimated by utilizing data of star particles and population synthesis code *PEGASE* (Fioc & Rocca-Volmerange 1999). Then,  $M_V = -19.8$  is obtained, so that the specific frequency defined as  $S_N = N_{cl} \times 10^{(M_V + 15)}$  (Harris & van den Bergh 1981) is 0.61. Here,  $N_{cl}$  is number of YMCs and  $N_{cl} = 49$ , and an effect of dust absorption is not taken into account. This value seems to be lower than that observed in dwarf ellipticals and is comparable to that of late-type galaxies (Miller et al. 1998). This is

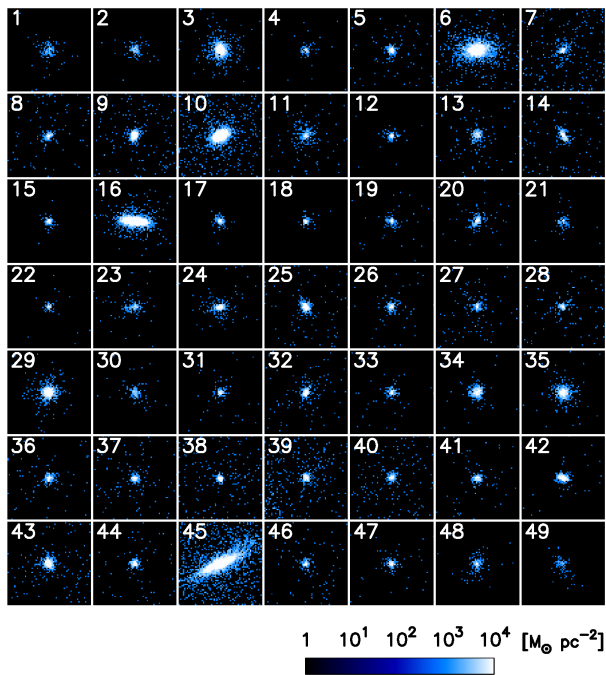


**Fig. 3.** Snapshots of detected YMCs. The size of each panel is 100 pc. The number displayed at upper left in each panel shows ID.

because only 300 Myr passes after galaxy-galaxy merging is completed and star particles are young so that the remnant is still bright. If star particles evolve further and the remnant becomes dark, the value is close to observed one. For example, when further 1000 Myr passes,  $M_V$  and  $S_N$  becomes  $-18.9$  and  $1.4$ , respectively, assuming passive evolution.

### 3.2 Distribution of young massive clusters

All detected YMCs are shown in figure 3. The physical quantities of the clusters are listed in Tab. 1. Figure 4 shows the fraction of YMCs and new stars in number as a function of radius from the galactic center. Most of YMCs are located at the region of a few kpc from the galactic center whereas new stars are extremely concentrated in the central region and nearly 40 % of them are distributed within 100 pc. In  $H_{TT}$  and  $L_{TT}$  cases, distribution of YMCs and new stars is similar to that of  $H_{TT,5pc}$  case as shown in figure 2 and table 2. The difference of distribution between YMCs and stars in the galactic central region is consistent with observations (Sikkema et al. 2006) and can be explained as follows. YMCs form mainly from widespread gas filaments generated at encounter of two galaxies or spatially extended turbulent gas generated by its inflow toward galactic central region at final coalescence phase of galactic cores. On the other hand, a large number of new stars are supplied by sinking of hypermassive

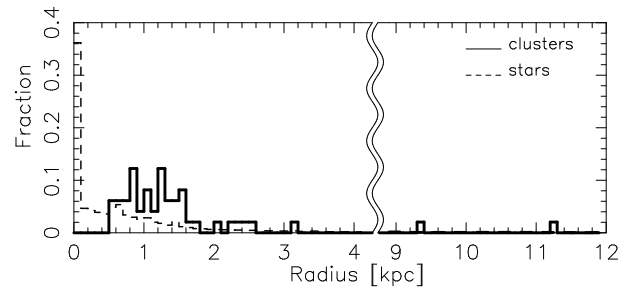


**Fig. 4.** Distribution of star clusters and new stars. The horizontal and vertical axes show radius from the center of the merger remnant and number fraction of them. The graph has a bin width of 100 pc.

star clusters in addition to star formations from such compressed gas (paper I). The formation epoch of YMCs in our simulations is different from Renaud et al. (2015) in which cluster formations are mainly take place at the first encounter of galaxies. This would be due to difference of collision parameters. In Renaud et al. (2015), Antennae-like collision parameter is adopted, which reproduces compression of gas and formation of star clusters after the first encounter of galaxies.

Two of clusters, of which ID is 48 and 49, appear at  $\sim 10$  kpc from the center of the merger remnant. These clusters are gravitationally bound by the remnant. Their formations take place in tidal tails apart from the center, which is different from formations of other clusters. These are classified as tidal dwarfs. In our simulations, there is no ejected YMC from the galaxy during galaxy-galaxy interaction as suggested by Elmegreen (2010). The difference of the formation site produces two component of YMC distribution. In  $H_{TT}$  and  $L_{TT}$  cases, formation of a tidal dwarf does not occur.

In order to compare our data with observations, we show the surface number density of YMCs as a function of radius from the galactic center in figure 5. Here, the surface density is calculated by using projected snapshots which are observed from various viewpoints. The figure shows that the distribution of YMCs do not strongly depend on viewing angle. Whereas the stellar distribution traces distribution of YMCs in the galactic outer region, the deficit of YMCs appears in the galactic inner region. This result is in agreement with observations of isolated elliptical galaxies (Sikkema et al. 2006; Salinas et al. 2015).

### 3.3 Mass function of young massive clusters

Cumulative mass function of YMCs is shown in figure 6. In  $H_{TT,5pc}$  model, the masses of clusters range from  $2.08 \times 10^5 M_\odot$  to  $4.51 \times 10^7 M_\odot$ . There are no hypermassive star clusters with  $\sim 10^8 M_\odot$  since they have al-

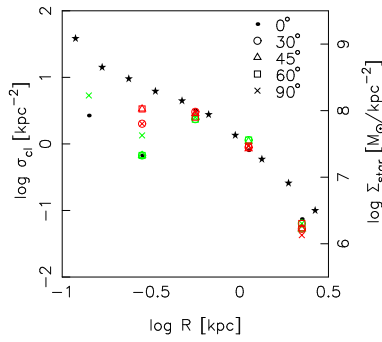


**Fig. 5.** Surface number density  $\sigma_{\text{cl}}$  of YMCs and surface new stellar mass density  $\Sigma_{\text{star}}$  as a function of radius from the galactic center. The bin width of  $\sigma_{\text{cl}}$  and  $\Sigma_{\text{star}}$  is 0.3, 0.15, respectively. In order to obtain projected snapshots from various viewpoints, we rotate figure 1 with respect to its horizontal or vertical axis. The red and green plots show the horizontal and vertical cases, respectively. The dots, circles, triangles, squares, and crosses denote  $\sigma_{\text{cl}}$  in  $0^\circ$ ,  $30^\circ$ ,  $45^\circ$ ,  $60^\circ$ , and  $90^\circ$  cases, respectively. The black star symbols denote  $\Sigma_{\text{star}}$ .

ready sunk to the galactic center through dynamical friction. This graph indicates that mass function becomes a power law function with  $dN/dM \propto M^{-2}$ , which is good agreement with observations (Whitmore et al. 1999) and previous numerical simulations (Saitoh et al. 2010).

A deviation from the line of  $dN/dM \propto M^{-2}$ , however, appears at  $\sim 10^7 M_\odot$ , in other words, there is an excess of massive clusters. The stellar mass evolutions of massive YMCs, of which IDs are 10, 16, and 45, are shown in figure 7. The figure shows that their initial stellar masses are less than  $\sim 10^7 M_\odot$ . After formations of YMCs, these 3 YMCs continue to pass filamentary dense gas regions which exist within  $\sim 1$  kpc from the galactic center. The YMCs obtain such dense gas continuously, and formations of new stars take place within YMCs. As a result, stellar mass growth of the YMCs occurs and the excess of massive YMCs emerges. Since the cluster with ID 16 escapes from the dense gas region, mass growth is quenched at  $t \sim 1030$  Myr. These objects seem to be spatially extended (see figure 3) than observed young clusters which have half light radius with a few pc (Mengel et al. 2008). Such massive clusters would sink into the galactic center through dynamical friction less than 1 Gyr according to Chandrasekhar's formula

$$t_{\text{dyn}} = \frac{0.95 \text{ Gyr}}{\ln \Lambda} \left( \frac{r}{0.5 \text{ kpc}} \right)^2 \frac{\sigma}{200 \text{ km s}^{-1}} \frac{2 \times 10^7 M_\odot}{M} \quad (1)$$

(Binney & Tremaine 1987). Then, the excess disappears and spatially extended clusters would not be observed.

In  $H_{\text{TT}}$  model, mass function in the less massive region than  $10^6 M_\odot$  is deviated from  $dN/dM \propto M^{-2}$ . This is because large gravitational softening length prevents from formations of clusters less than  $10^6 M_\odot$ .

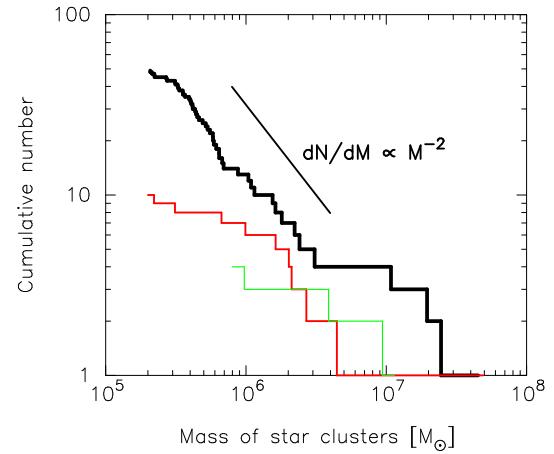


**Fig. 6.** Cumulative mass function. The horizontal and vertical axes are cumulative number and mass of YMCs, respectively. The black, red, green lines show  $H_{\text{TT},5\text{pc}}$ ,  $H_{\text{TT}}$ ,  $L_{\text{TT}}$ , respectively.

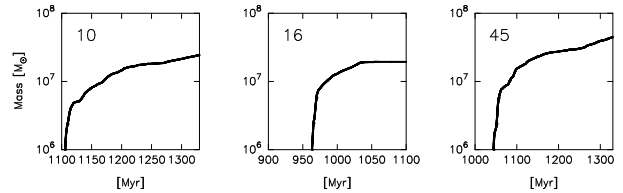


**Fig. 7.** Time evolution of stellar mass of massive YMCs, of which IDs are 10, 16, and 45 respectively.

### 3.4 Age of young massive clusters

In table 1,  $t_{\text{XX}\%}$  indicates the time when XX% of stars in each cluster are formed. According to  $t_{25\%}$ ,  $t_{50\%}$ , and  $t_{75\%}$ , the clusters are able to be classified into the following three types: (1) clusters consisting of only new stars with single age, (2) clusters consisting of only new stars with bimodal distribution in age, (3) massive clusters consisting of only new stars with various age, and (4) clusters constituting of both new and old stars.

Thirty eight YMCs consist of only new stars with single age. All of these clusters form after galaxy-galaxy encounter, and their formations are induced by the galaxy merger. The typical population of stellar age within these clusters is shown in the left panel of figure 8 which shows number fraction of stars within a cluster as a function of star formation time. Stars within these clusters have similar formation epoch and the width of age distribution is 10 Myr which is timescale of feedback to eject gas.

One YMC, of which ID is 25, has bimodal distribution in age as shown in the middle panel of figure 8. The interval of age between two events is 200 Myr. The process of producing such population is as follows. The cluster forms at  $t = 1050$  Myr. After the formation, the cluster wanders few gas region. When the cluster passes the dense gas

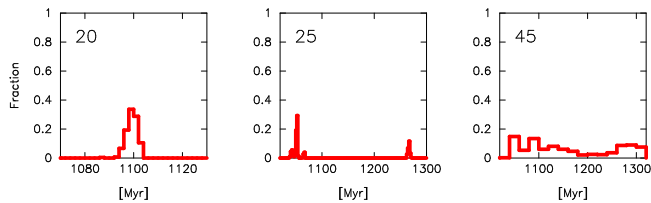


**Fig. 8.** Distribution of star formation time in each YMC formed after the galaxy encounter. The horizontal and vertical axes are star formation time and number fraction of stars to total stellar number, respectively. The number at upper-left denotes cluster ID.

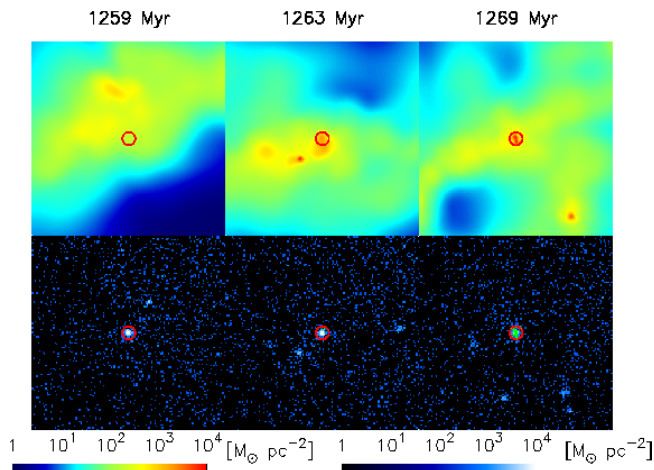


**Fig. 9.** Snapshots of the cluster with ID 25 from  $t = 1259$  Myr to  $t = 1269$  Myr. Above and bottom panels show surface density of gas and new star, respectively. The red circle represents the position of the cluster. In bottom panels, green dots represent formed next generation stars. At  $t = 1259$ , dense gas region appears above the cluster. After that, the cluster pass through this region. Then, the cluster captures gas at  $t = 1263$  Myr and star formation takes place within the cluster.

region temporarily after  $t \sim 1250$  Myr, it captures gas as shown in the left and middle panels of figure 9. After that, the density of gas within the cluster becomes high and gas cools because of radiative cooling. As a result, the next generation stars form as shown in the right panel of figure 9.

Three YMCs, of which IDs are 10, 16, and 45, exceed  $10^7 M_{\odot}$ . These clusters consist of stars with various ages. The typical distribution of the stellar formation time is shown in the right panel of figure 8. The distribution is rather continuous than discrete unlike ID 25. This is because these YMCs continue to pass dense gas region and obtain gas continuously. The continuous gas accretion results in star formations within the clusters at various time.

The other 7 YMCs consist of old and new stars although clusters, of which IDs are 1 and 34, have few new stars. All of these 7 clusters form in an initial unstable gas disk at  $t \sim -800$  Myr during a simulation of an isolated gas disk. Figure 10 shows distribution of formation time of stars

within these clusters. Although these clusters form in an initial isolated unstable gas disk at  $t \sim -800$  Myr, they include stars with various formation time. This is because clusters capture gas when they pass through dense gas region and star formations occur within them similarly to the cluster of ID 25. These clusters are likely to contain stars formed at the encounter phase, namely around 400 Myr or 800 Myr. The reason is that the encounter produces turbulent and dense gas and increases the probability that a cluster passes through the dense gas region.

In  $H_{TT}$  and  $L_{TT}$  cases,  $t_{25\%}$ ,  $t_{50\%}$ , and  $t_{75\%}$  are shown in table 2. All YMCs form after the second encounter of galaxies. Whereas most YMCs have single stellar population, ID 50, 61, and 62 has multiple stellar populations. ID 50 and 62 consist of stars with various ages similarly to ID 10, 16, and 45, and ID 61 has bimodal stellar population in age similarly to ID 25. The multiple population is formed by capturing dense gas and forming the second generation stars similarly to the  $H_{TT,5pc}$  case.

Recent observations have revealed that Galactic globular clusters generally have multiple stellar populations (Bastian & Lardo 2017). Such globular clusters can be divided into two types in accordance with abundance patterns. The first and second types contain Fe and light element (e.g., He, C, N, O, Na, and Al) variations, respectively. Since we do not have abundance information for stars in our simulation, we conjecture types of YMCs with bimodal distribution in age. These YMCs should belong to the first type in the following reason. These YMCs except ID 25 contains stellar populations formed before and after the galaxy-galaxy merger. These stellar populations clearly have different Fe abundance. The YMC with ID 25 has stellar populations formed at  $t \sim 1050$  Myr and  $t \sim 1250$  Myr. The metallicity,  $Z$ , of the first and second generation stars in the YMC with ID 25 is shown in figure 11. The figure shows that metallicity of the second generation stars increases by  $\sim 0.01$  compared to that of first generation stars. Although the enrichment seems to be mild, it becomes more remarkable in high- $z$  galaxies with low metallicity. The difference of metallicity between the first and the second generation stars indicates that the second generation stars form from gas contaminated by TypeII SNe. Thus, these clusters correspond to  $\omega$  Cen with different Fe abundance. On the other hand, the second type is expected to be formed from asymptotic giant branch (AGB) ejecta of the first generation stars (Renzini 2008; Bekki et al. 2017; Bekki 2018).

**Table 1.** Property of YMCs in the  $H_{\text{TT},5\text{pc}}$  case.

ID	$M [M_{\odot}]^*$	$r [\text{kpc}]^{\dagger}$	$t_{25\%} [\text{Myr}]^{\ddagger}$	$t_{50\%} [\text{Myr}]^{\S}$	$t_{75\%} [\text{Myr}]^{\parallel}$	$r_{\text{p}}^{\#}$	$r_{\text{a}}^{**}$	$\epsilon^{\dagger\dagger}$
1	$3.14 \times 10^5$	2.01	-779	-778	-703	1.88	2.03	0.04
2	$3.12 \times 10^5$	2.40	-845	-843	146	1.58	2.63	0.25
3	$3.09 \times 10^6$	1.55	-369	298	832	0.65	1.69	0.45
4	$2.23 \times 10^5$	1.38	742	743	744	1.37	1.82	0.14
5	$6.43 \times 10^5$	0.81	1061	1062	1063	0.44	0.85	0.31
6	$1.08 \times 10^7$	1.08	978	984	987	0.62	1.29	0.35
7	$4.41 \times 10^5$	0.64	1238	1239	1240	0.55	0.68	0.11
8	$4.02 \times 10^5$	0.88	1182	1183	1185	0.59	0.90	0.21
9	$2.22 \times 10^6$	0.54	1030	1030	1032	0.53	0.88	0.25
10	$2.46 \times 10^7$	0.58	1136	1180	1254	0.58	0.59	0.01
11	$5.53 \times 10^5$	1.24	1181	1182	1183	1.05	1.32	0.11
12	$3.68 \times 10^5$	1.58	1151	1153	1154	0.98	1.60	0.24
13	$4.34 \times 10^5$	0.83	967	970	971	0.79	1.38	0.28
14	$5.90 \times 10^5$	0.71	1068	1069	1070	0.60	0.74	0.10
15	$4.17 \times 10^5$	2.39	1033	1034	1035	0.57	2.40	0.62
16	$1.95 \times 10^7$	1.41	969	984	1011	0.25	1.70	0.75
17	$3.93 \times 10^5$	2.51	952	953	954	1.02	2.54	0.43
18	$3.28 \times 10^5$	2.29	705	706	707	0.95	2.72	0.48
19	$3.26 \times 10^5$	1.21	1267	1268	1269	0.49	1.28	0.45
20	$6.14 \times 10^5$	1.41	1098	1099	1101	0.83	1.46	0.27
21	$2.22 \times 10^5$	1.36	1093	1102	1105	0.65	1.48	0.39
22	$2.14 \times 10^5$	1.73	1058	1059	1060	1.21	1.86	0.21
23	$3.55 \times 10^5$	1.24	1278	1279	1280	0.98	1.24	0.12
24	$1.04 \times 10^6$	1.57	1100	1102	1104	0.96	1.58	0.25
25	$1.15 \times 10^6$	0.88	1051	1053	1259	0.83	0.89	0.04
26	$4.62 \times 10^5$	1.17	1166	1168	1169	0.84	1.23	0.19
27	$3.54 \times 10^5$	1.05	1266	1269	1270	0.87	1.16	0.15
28	$5.17 \times 10^5$	1.04	1318	1319	1321	0.89	1.12	0.11
29	$2.41 \times 10^6$	3.17	-558	14	487	0.61	3.39	0.70
30	$2.71 \times 10^5$	1.32	-839	-111	416	1.26	3.78	0.50
31	$2.74 \times 10^5$	1.16	1154	1155	1157	0.82	1.23	0.20
32	$8.76 \times 10^5$	0.91	1147	1149	1150	0.91	1.04	0.07
33	$4.16 \times 10^5$	1.24	1115	1116	1117	0.73	1.24	0.26
34	$1.09 \times 10^6$	1.50	-872	-870	-869	0.25	1.67	0.74
35	$1.55 \times 10^6$	1.50	-871	-869	472	0.92	2.88	0.52
36	$5.33 \times 10^5$	0.88	1182	1184	1185	0.62	0.91	0.19
37	$5.81 \times 10^5$	0.78	1062	1063	1064	0.59	0.82	0.16
38	$6.77 \times 10^5$	0.62	1197	1198	1199	0.31	0.71	0.40
39	$6.44 \times 10^5$	0.80	1231	1232	1234	0.58	0.88	0.21
40	$5.82 \times 10^5$	0.90	1060	1061	1061	0.67	0.95	0.17
41	$4.49 \times 10^5$	1.21	1169	1171	1172	1.13	1.29	0.06
42	$1.62 \times 10^6$	1.62	950	950	951	0.32	3.47	0.83
43	$1.80 \times 10^6$	0.53	1017	1019	1019	0.36	0.91	0.44
44	$6.93 \times 10^5$	0.74	1022	1023	1023	0.26	1.59	0.72
45	$4.51 \times 10^7$	0.69	1087	1145	1269	0.69	0.78	0.06
46	$3.34 \times 10^5$	1.02	1176	1177	1178	0.94	1.39	0.19
47	$4.91 \times 10^5$	1.25	875	876	876	0.62	1.42	0.39
48	$4.07 \times 10^5$	11.30	817	819	820	11.04	18.67	0.26
49	$2.08 \times 10^5$	9.31	762	765	766	9.07	17.63	0.32

\* Mass of a YMC.

 $\dagger$  Distance of a YMC from the center of the merger remnant. $\ddagger$  Star formation time of a star located at 25% when stars within a YMC are sorted from young to old. $\S$  Star formation time of a star located at 50% when stars within a YMC are sorted from young to old. $\parallel$  Star formation time of a star located at 75% when stars within a YMC are sorted from young to old. $\#$  Pericenter distance of a YMC. $**$  Apocenter distance of a YMC. $\dagger\dagger$  Eccentricity of an orbit.

**Table 2.** Property of YMCs in  $H_{TT}$  and  $L_{TT}$  cases. YMCs from ID 50 to ID 59 and from ID 60 to ID 63 form in  $H_{TT}$  and  $L_{TT}$  cases, respectively.

ID	$M [M_{\odot}]^*$	$r$ [kpc] <sup>†</sup>	$t_{25\%}$ [Myr] <sup>‡</sup>	$t_{50\%}$ [Myr] <sup>§</sup>	$t_{75\%}$ [Myr] <sup>  </sup>	$r_p$ <sup>‡</sup>	$r_a$ <sup>**</sup>	$\epsilon$ <sup>††</sup>
50	$4.90 \times 10^7$	0.41	898	917	969	0.38	1.28	0.54
51	$2.21 \times 10^5$	1.15	1173	1175	1177	1.09	1.22	0.06
52	$2.02 \times 10^6$	1.06	1164	1166	1168	1.05	1.10	0.02
53	$6.69 \times 10^5$	0.73	1195	1197	1198	0.69	0.73	0.03
54	$1.63 \times 10^6$	2.97	897	901	903	0.08	3.03	0.95
55	$9.90 \times 10^5$	1.37	917	918	919	0.77	1.43	0.30
56	$4.45 \times 10^6$	1.16	889	897	900	0.75	1.46	0.32
57	$2.69 \times 10^6$	0.84	1000	1001	1002	0.34	0.87	0.43
58	$3.12 \times 10^5$	1.19	888	895	899	0.75	1.44	0.31
59	$2.11 \times 10^6$	0.95	1025	1026	1027	0.94	1.08	0.07
60	$9.40 \times 10^6$	1.21	1011	1015	1020	0.82	1.21	0.19
61	$1.14 \times 10^7$	0.91	1200	1203	1314	0.75	0.91	0.10
62	$3.88 \times 10^6$	2.24	883	885	913	0.17	3.44	0.91
63	$9.72 \times 10^5$	0.90	1214	1215	1217	0.90	1.13	0.11

\* Mass of a YMC.

† Distance of a YMC from the center of the merger remnant.

‡ Star formation time of a star located at 25% when stars within a YMC are sorted from young to old.

§ Star formation time of a star located at 50% when stars within a YMC are sorted from young to old.

|| Star formation time of a star located at 75% when stars within a YMC are sorted from young to old.

‡ Pericenter distance of a YMC.

\*\* Apocenter distance of a YMC.

†† Eccentricity of an orbit.

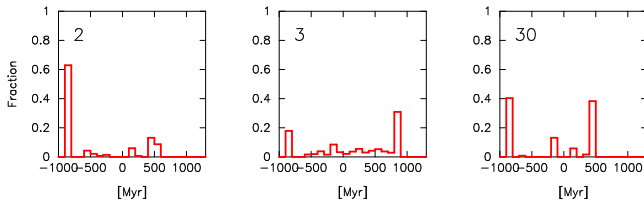


**Fig. 10.** Same as figure 8 but clusters formed before the galaxy encounter.

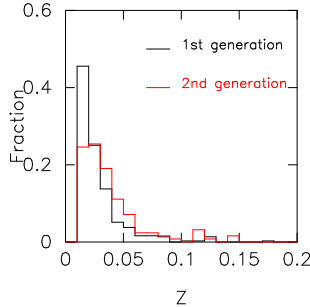


**Fig. 11.** The number fraction of stars as a function of metallicity  $Z$  in the cluster with ID 25. The black and red lines show the first and the second generation stars, respectively. The bin width is 0.01.

### 3.5 Motion of young massive clusters

In order to investigate orbits of YMCs in the merger remnant, we simulate motion of YMCs by the second order leapfrog integration scheme. The gravitational potential of the remnant is produced by using distribution of SPH, star, and dark matter particles at  $t \sim 1350$  Myr. Here, we assume that the gravitational potential is steady and spherically symmetry. These assumptions are reasonable

to calculate orbits approximately since asymmetry of the remnant is not strong and the remnant is quasi-stable. Note that evaporation of YMCs and dynamical friction are not taken account.

The pericenter distance  $r_p$ , apocenter distance  $r_a$ , and eccentricity defined by  $\epsilon = (r_a - r_p)/(r_a + r_p)$  are summarized in table 1 for the high resolution case and in table 2 for the low resolution cases. In both cases, orbits of YMCs in the galactic inner region are various, but the number fraction of circular orbits is large. This is because YMCs formed in a major merger do not lose the orbital angular momentum sufficiently. This trend seems to be different from observations of Milky Way (Gaia Collaboration et al. 2018) or cosmological simulations of a disk galaxy (Saitoh et al. 2006) which is different morphology from a galaxy-galaxy merger remnant and do not experience a recent major merger. Such observations and simulations show that a large fraction of YMCs have radial orbits. This might indicate that formation process of clusters is different between a merging galaxy and a disk galaxy. While YMCs form from filamentary gas or turbulent gas generated by a galaxy-galaxy merger, YMCs form by in situ formation, minor mergers, and satellite accretion (Renaud et al. 2017).

Eccentricities of orbits of the galactic outer YMCs, of which ID are 48 and 49, are not high. This is because they form in rotating tidal tails and hence have originally sufficient orbital angular momentum. These clusters migrate from  $\sim 10$  kpc to  $\sim 20$  kpc. Since their pericenter and apocenter distance are  $\sim 10$  kpc and  $\sim 20$  kpc, respectively, these objects are observed as isolated globular



clusters. The isolated globular clusters are observed in some galaxies, for examples M31 (Mackey et al. 2010) and M81 (Jang et al. 2012), although it is difficult to compare simply with spiral galaxies.

## 4 Summary

We investigate properties of YMCs in a merger remnant by analyzing simulation data in paper I. Our findings are as follows.

- YMCs are formed in filamentary and turbulent gas and tidal tails generated by a galaxy merger. The former and the latter are distributed at a few kpc and at  $\sim 10$  kpc from the center of the merger remnant, respectively. The YMCs are much less concentrated than galaxy stars.
- The mass function of YMCs becomes  $dN/dM \propto M^{-2}$ , but the excess appears around  $10^7 M_{\odot}$  after merging of galactic cores is completed. The excess would disappear less than 1 Gyr due to dynamical friction.
- Most of YMCs formed during a galaxy merger consist of single stellar population in age. On the other hand, the rest have multiple distribution in age. The multiple population is formed by capturing dense gas and forming new stars within a YMC when a YMC pass dense gas region.
- Orbits of YMCs in the inner galactic region are various, but large fraction of candidates would rather have circular orbits. Eccentricities of YMCs in the inner galactic region are not high.

We thank Dr. Florent Renaud for giving us useful comments. Numerical computations were carried out on Cray XT4 at Center for Computational Astrophysics (CfCA), National Astronomical Observatory of Japan, and numerical analyses were carried out on computers at CfCA, National Astronomical Observatory of Japan. This research has been supported in part by the MEXT programme for the Development and Improvement for the Next Generation Ultra High-Speed Computer System under its Subsidies for Operating the Specific Advanced Large Research Facilities, and by Grants-in-Aid for Scientific Research (16K17656, 17H06360) from the Japan Society for the Promotion of Science.

## References

Barnes, J. E., & Hernquist, L. 1996, *ApJ*, 471, 115  
 Bassino, L. P., & Caso, J. P. 2017, *MNRAS*, 466, 4259  
 Bastian, N., & Lardo, C. 2017, *ArXiv e-prints*, arXiv:1712.01286  
 Bekki, K. 2018, *ArXiv e-prints*, arXiv:1807.02309  
 Bekki, K., Forbes, D. A., Beasley, M. A., & Couch, W. J. 2002,

*MNRAS*, 335, 1176  
 Bekki, K., Jeřábková, T., & Kroupa, P. 2017, *MNRAS*, 471, 2242  
 Binney, J., & Tremaine, S. 1987, *Galactic dynamics*  
 Bournaud, F., Duc, P.-A., & Emsellem, E. 2008, *MNRAS*, 389, L8  
 Choudhury, S., Subramaniam, A., & Cole, A. A. 2016, *MNRAS*, 455, 1855  
 Cox, T. J., Dutta, S. N., Di Matteo, T., et al. 2006, *ApJ*, 650, 791  
 Di Matteo, P., Combes, F., Melchior, A.-L., & Semelin, B. 2007, *A&A*, 468, 61  
 Elmegreen, B. G. 2010, *ApJL*, 712, L184  
 Fioc, M., & Rocca-Volmerange, B. 1999, *ArXiv Astrophysics e-prints*, astro-ph/9912179  
 Gaia Collaboration, Helmi, A., van Leeuwen, F., et al. 2018, *ArXiv e-prints*, arXiv:1804.09381  
 Harris, W. E., & van den Bergh, S. 1981, *AJ*, 86, 1627  
 Hopkins, P. F., Cox, T. J., Hernquist, L., et al. 2013a, *MNRAS*, 430, 1901  
 Hopkins, P. F., Kereš, D., Murray, N., et al. 2013b, *MNRAS*, 433, 78  
 Jang, I. S., Lim, S., Park, H. S., & Lee, M. G. 2012, *ApJL*, 751, L19  
 Kaneko, H., Kuno, N., & Saitoh, T. R. 2018, *ArXiv e-prints*, arXiv:1805.11630  
 Kazantzidis, S., Mayer, L., Colpi, M., et al. 2005, *ApJL*, 623, L67  
 Kim, J.-h., Wise, J. H., & Abel, T. 2009, *ApJL*, 694, L123  
 Kim, J.-h., Ma, X., Grudić, M. Y., et al. 2018, *MNRAS*, 474, 4232  
 Ko, Y., Lee, M. G., Park, H. S., et al. 2018, *ApJ*, 859, 108  
 Kruijssen, J. M. D., Pelupessy, F. I., Lamers, H. J. G. L. M., et al. 2012, *MNRAS*, 421, 1927  
 Mackey, A. D., Ferguson, A. M. N., Irwin, M. J., et al. 2010, *MNRAS*, 401, 533  
 Makino, J., Akiyama, K., & Sugimoto, D. 1990, *PASJ*, 42, 205  
 Mao, M. Y., Norris, R. P., Emonts, B., et al. 2014, *MNRAS*, 440, L31  
 Matsui, H., Saitoh, T. R., Makino, J., et al. 2012, *ApJ*, 746, 26  
 Mengel, S., Lehnert, M. D., Thatte, N. A., et al. 2008, *A&A*, 489, 1091  
 Mihos, J. C., & Hernquist, L. 1996, *ApJ*, 464, 641  
 Miller, B. W., Lotz, J. M., Ferguson, H. C., Stiavelli, M., & Whitmore, B. C. 1998, *ApJL*, 508, L133  
 Renaud, F., Agertz, O., & Gieles, M. 2017, *MNRAS*, 465, 3622  
 Renaud, F., Bournaud, F., & Duc, P.-A. 2015, *MNRAS*, 446, 2038  
 Renzini, A. 2008, *MNRAS*, 391, 354  
 Saitoh, T. R., Daisaka, H., Kokubo, E., et al. 2010, in *Astronomical Society of the Pacific Conference Series*, Vol. 423, *Galaxy Wars: Stellar Populations and Star Formation in Interacting Galaxies*, ed. B. Smith, J. Higdon, S. Higdon, & N. Bastian, 185  
 Saitoh, T. R., Daisaka, H., Kokubo, E., et al. 2008, *PASJ*, 60, 667  
 —. 2009, *PASJ*, 61, 481

- Saitoh, T. R., Koda, J., Okamoto, T., Wada, K., & Habe, A. 2006, *ApJ*, 640, 22
- Salinas, R., Alabi, A., Richtler, T., & Lane, R. R. 2015, *A&A*, 577, A59
- Sikkema, G., Peletier, R. F., Carter, D., Valentijn, E. A., & Balcells, M. 2006, *A&A*, 458, 53
- Soifer, B. T., Neugebauer, G., Matthews, K., et al. 2000, *AJ*, 119, 509
- Steinmetz, M., & Mueller, E. 1994, *A&A*, 281, L97
- Teyssier, R., Chapon, D., & Bournaud, F. 2010, *ApJL*, 720, L149
- Whitmore, B. C., & Schweizer, F. 1995, *AJ*, 109, 960
- Whitmore, B. C., Zhang, Q., Leitherer, C., et al. 1999, *AJ*, 118, 1551